JOURNAL OF COMPUTATIONAL PHYSICS **134,** 296–305 (1997)
ARTICLE NO. CP975708

Ultrarelativistic SPH

E. Chow and J. J. Monaghan

Department of Mathematics, Monash University, Clayton Victoria 3168, Australia
E-mail: jjm@sapphire.maths.monash.edu.au

Received July 22, 1996; revised March 18, 1997

In this paper the equations of motion of an ultrarelativistic gas are solved using the particle method SPH. The algorithm is based on a form of SPH which integrates the specific energy equation instead of the thermal energy equation and determines the dissipative terms along the lines of Riemann solvers. The resulting algorithms give good results for strongly relativistic shock tubes and they can handle collisions with relativistic velocities at least 0.9999 the speed of light. Because the method uses a resolution which varies with time and in space it appears ideal for the simulation of collisions between ultrarelativistic nuclei. © 1997 Academic Press

1. INTRODUCTION

The numerical study of relativistic fluid dynamics is a key element in the study of physical systems as diverse as astrophysical jets [1] and the collision of heavy ion nuclei [3]. However, it is only recently that satisfactory numerical methods have become available for relativistic gas dynamics. It was initially thought that a fully implicit method would be needed for ultrarelativistic gas dynamics [23] but recent work on Riemann methods [15–17] and upwind and FCT methods [25] has given good results for shock tubes, blast waves, and relativistic jets [18, 19].

Despite these results the finite difference solutions based in whole or part on Riemann solutions have disadvantages [29, 30]. The first of these is that the Riemann problem must be solved. In the nonrelativistic case approximations [4] can be used but, in more complicated problems, the solution of the Riemann problem can be a substantial undertaking. For example, while there are solutions for the ideal relativistic gas [16, 17], there are no solutions yet available for the Riemann problem for relativistic gases using the correct relativistic equation of state and allowing new particle species to be produced during the evolution. The situation in more than one dimension is worse because many more basic states become possible. For example, in the simple case of an isentropic, two-dimensional, nonrelativistic Riemann problem where four constant states meet at a common corner there are 16 different possible configurations (77 if the discontinuities are across two nonparallel lines), and some of these are unstable [26]. Fortunately the higher dimensional ideal gas Riemann problem can be approximated accurately by a succession of one-dimensional problems [6, 9, 18, 19], although it is not clear what the situation is for more complicated systems. A further consideration, relevant to the collision of nuclei, is that some Riemann methods do not easily handle those flows where large regions with low density are generated (for example, linear Riemann solvers may fail for strong rarefaction waves as in the Sjögreen test [8, 29] or the high Mach number impulsive start of a cylinder [32]. The flux rules of Donat and Maquina [5] are more robust, especially the first-order algorithm but, to counter the excessive smearing of contact discontinuities which this gives, a third-order algorithm must be used. This third-order algorithm fails for some examples of the Sjögreen test. A further disadvantage of the Riemann methods is that they cannot be generalized easily to include adaptive resolution. For these reasons it seems appropriate to explore more flexible algorithms for relativistic fluid dynamics.

Particle methods such as SPH (for a review see [20]) have advantages in collision problems because the particles are concentrated with the material thus increasing the efficiency of the calculation. Furthermore, the resolution can be made adaptive in space and time with little effort. Early SPH applications to relativistic flows produced satisfactory results but the problems considered were only mildly relativistic [12, 14] and when applied to ultra relativistic flows they broke down. Part of the difficulty is that an artificial viscosity is required and it is not clear what form it should take [11, 21]. The problems are made more acute because the standard dissipative terms [7, 13] are known to be unstable [10, 24].

Improvements to the standard SPH algorithms, particularly through changes to the dissipation terms and the integration of the specific energy equation, instead of the thermal energy equation, give very good results for nonrelativistic shock tubes. In this paper we generalize these algorithms to produce relativistic SPH equations which are based on the conservation equations for momentum and energy. The dissipative terms are constructed in analogy to terms in the Riemann methods with very good results

0021-9991/97 $25.00

for highly relativistic fluid flows. The particle algorithm seems to be ideal for the study of collisions of heavy ion nuclei.

2. THE RELATIVISTIC EQUATIONS OF MOTION

We begin with the equations of motion of a nondissipative fluid [13] which, for convenience, we assume is composed of baryons. The Eulerian equations of motion for the laboratory baryon number density N, momentum $\mathbf{M}$, and energy E are:

Continuity,

$$\frac{\partial N}{\partial t} + \frac{\partial (N v^j)}{\partial x^j} = 0; \tag{2.1}$$

Momentum,

$$\frac{\partial M^i}{\partial t} + \frac{\partial (M^i v^j)}{\partial x^j} = -\frac{\partial P}{\partial x^j}\delta^{ij}; \tag{2.2}$$

Energy,

$$\frac{\partial E}{\partial t} + \frac{\partial}{\partial x^j}((E+P)v^j) = 0, \tag{2.3}$$

where

$$M^j = v^j \gamma^2 (P + X)/c^2, \tag{2.4}$$

$$E = \gamma^2 (P + X) - P, \tag{2.5}$$

and

$$X = n m_0 c^2 + nu. \tag{2.6}$$

In these equations c is the speed of light, m_0 is the rest mass of a baryon, n is the baryon number density in the local frame of an element of fluid (so that $N = \gamma n$), u is the internal energy in the local frame, and

$$\gamma = \frac{1}{\sqrt{1 - v^2/c^2}}. \tag{2.7}$$

$\mathbf{M}$ and E are the momentum and energy per unit volume. In order to set up the SPH equations we need momentum and energy per particle. The momentum per particle $\mathbf{q}$ and energy per particle $\hat{e}$ are given by

$$\mathbf{q} = \frac{\mathbf{M}}{N} = \mathbf{v}\gamma\left(1 + u + \frac{P}{n}\right) \tag{2.8}$$

and

$$\hat{e} = \frac{E}{N} = \gamma\left(1 + u + \frac{P}{n}\right) - \frac{P}{N}, \tag{2.9}$$

where all energies and P/n are measured in units of $m_0 c^2$ and, in the following, the unit of velocity is c.

Using these definitions we find

$$\frac{d\mathbf{q}}{dt} = -\frac{1}{N}\nabla P \tag{2.10}$$

and

$$\frac{d\hat{e}}{dt} = -\frac{1}{N}\nabla \cdot (P\mathbf{v}), \tag{2.11}$$

where

$$\frac{d}{dt} = \frac{\partial}{\partial t} + \mathbf{v}\cdot\nabla.$$

Particles are moved according to

$$\frac{d\mathbf{r}}{dt} = \mathbf{v}. \tag{2.12}$$

These Lagrangian equations are identical in form to their nonrelativistic counterparts and they can be solved in a similar way.

3. THE RELATIVISTIC SPH EQUATIONS

The usual forms of the SPH equations [20] can be taken over, except that each SPH particle b carries ν_b baryons instead of mass m_b. The continuity and momentum equations for particle a can then be written

$$\frac{dN_a}{dt} = \sum_b \nu_b (\mathbf{v}_a - \mathbf{v}_b)\cdot\nabla_a W_{ab} \tag{3.1}$$

and

$$\frac{d\mathbf{q}_a}{dt} = -\sum_b \nu_b \left(\frac{P_a}{N_a^2} + \frac{P_b}{N_b^2} + \Pi_{ab}\right)\nabla_a W_{ab}, \tag{3.2}$$

where we have included a dissipative term Π_{ab} (symmetric in a and b) which we will discuss below. The interpolating kernel W_{ab} is a function of $|\mathbf{r}_a - \mathbf{r}_b|$ so that its gradient can be written

$$\nabla_a W_{ab} = \mathbf{r}_{ab} F_{ab}, \tag{3.3}$$

where F_{ab} is a negative scalar function which is symmetric

in a and b and $\mathbf{r}_{ab}$ denotes $(\mathbf{r}_a - \mathbf{r}_b)$. This notation for vectors is used throughout this paper.

From these properties of $\nabla_a W_{ab}$ the interactions between particles are antisymmetric and along their line of centres. Linear and angular momentum

$$\sum_a \nu_a \mathbf{q}_a \quad \text{and} \quad \sum_a \nu_a \mathbf{r}_a \times \mathbf{q}_a, \tag{3.4}$$

are therefore conserved.

It is usual in SPH calculations to work with the internal energy equation rather than specific energy equation (2.11). However, recent nonrelativistic calculations [22] show that there are advantages in using (2.11) since the dissipative terms can be guided by the terms arising from Riemann solutions. In the relativistic case a further advantage of (2.11) is that, compared with the thermal energy equation, it does not involve time derivatives of γ.

One SPH form of (2.11) is obtained by first writing

$$\frac{\nabla \cdot (P\mathbf{v})}{N} = \mathbf{v} \cdot \nabla \left(\frac{P}{N}\right) + \frac{P}{N^2} \nabla \cdot (N\mathbf{v}), \tag{3.5}$$

from which we deduce

$$\frac{d\hat{e}_a}{dt} = -\sum_b \nu_b \left(\frac{P_a \mathbf{v}_b}{N_a^2} + \frac{P_b \mathbf{v}_a}{N_b^2} + \Omega_{ab}\right) \cdot \nabla_a W_{ab}, \tag{3.6}$$

and we have included a dissipative term Ω_{ab}, symmetric in a and b, which we will discuss below. The total energy,

$$E = \sum_a \nu_a \hat{e}_a, \tag{3.7}$$

is conserved.

4. RELATION TO RIEMANN SOLUTIONS

The Riemann method of Marti *et al.* [15] provides a convenient basis for the construction of Π_{ab} and Ω_{ab}. Starting with the equation written in conservation form,

$$\frac{\partial \mathbf{s}}{\partial t} + \frac{\partial \mathbf{f}}{\partial x} = 0, \tag{4.1}$$

a simple Euler scheme for their numerical solution is

$$\mathbf{s}_j^{n+1} = \mathbf{s}_j^n - \frac{\Delta t}{\Delta x}\left(\tilde{\mathbf{f}}(\mathbf{s}_j, \mathbf{s}_{j+1}) - \tilde{\mathbf{f}}(\mathbf{s}_{j-1}, \mathbf{s}_j)\right), \tag{4.2}$$

Marti *et al.* [15] define numerical fluxes by

$$\tilde{\mathbf{f}}(\mathbf{s}_L, \mathbf{s}_R) = \frac{1}{2}\left(\mathbf{f}_L + \mathbf{f}_R - \sum_{i=1}^{3} |\tilde{\lambda}_i| \, \Delta\tilde{\omega}_i \tilde{\mathbf{e}}_i\right), \tag{4.3}$$

where L and R stand for the left and right states at a given interface. The λ_i are the eigenvalues, and $\mathbf{e}_i$ are the eigenvectors of the Jacobian matrix,

$$\mathbf{A} = \frac{\partial \mathbf{f}(\mathbf{s})}{\partial \mathbf{s}}, \tag{4.4}$$

and $\tilde{\lambda}_i$ denotes an average of λ for the left and right states. The quantities $\Delta\omega$ are the jumps of the independent variables across the characteristics and they are given by

$$\mathbf{s}_R - \mathbf{s}_L = \sum_{i=1}^{3} \Delta\tilde{\omega}_i \tilde{\mathbf{e}}_i. \tag{4.5}$$

For relativistic ideal gases the eigenvalues for one-dimensional problems are v and $(v \pm c_s)/(1 \pm vc_s)$, where c_s is the speed of sound. These last two are the speed of propagation of sound waves against and with the gas flow as seen in the computing frame.

To construct an appropriate form of Π_{ab} for the interaction between particles a and b we treat them as the equivalent of left and right states taken with reference to the line joining the two particles. With (4.2) and (4.3) in mind we need the equivalent of the eigenvalues and a jump in the relevant physical variable, in this case the momentum. A first choice for Π_{ab} might then be

$$\Pi_{ab} = -\frac{K v_{\text{sig}} (\mathbf{q}_a - \mathbf{q}_b) \cdot \mathbf{j}}{\overline{N}_{ab}}, \tag{4.6}$$

where K is a dimensionless parameter ~ 1, $\overline{N}_{ab} = (N_a + N_b)/2$, v_{sig} is an appropriate signal velocity (see Section 5 below), and

$$\mathbf{j} = \frac{\mathbf{r}_{ab}}{|\mathbf{r}_{ab}|} \tag{4.7}$$

is the unit vector from b to a. However, to guarantee that the viscous dissipation of a gas is positive definite, it is necessary to replace $\mathbf{q}$ by

$$\mathbf{q}^* = \gamma^* \mathbf{v}\left(1 + u + \frac{P}{n}\right), \tag{4.8}$$

where

$$\gamma^* = \frac{1}{\sqrt{1 - (\mathbf{v} \cdot \mathbf{j})^2}}. \tag{4.9}$$

The reader is warned that in this paper the superscript * denotes that the variable involves $\mathbf{v}\cdot\mathbf{j}$ the line of sight velocity.

The final form for Π_{ab} is

$$\Pi_{ab} = -\frac{Kv_{\rm sig}(\mathbf{q}_a^* - \mathbf{q}_b^*)\cdot\mathbf{j}}{\overline{N}_{ab}}, \tag{4.10}$$

when particles a and b are approaching; otherwise $\Pi_{ab} = 0$. The reader will notice that our expression for Π_{ab} is symmetric in a and b and it is similar to the usual viscous dissipation term used in SPH.

In the same way, if a and b are approaching, we assume

$$\Omega_{ab} = -\frac{Kv_{\rm sig}(e_a^* - e_b^*)\mathbf{j}}{\overline{N}_{ab}}, \tag{4.11}$$

where we have replaced $\hat{e}$ by e^* which is identical to $\hat{e}$ except that γ is replaced by γ^*. We set $\Omega_{ab} = 0$ if the particles a and b are separating.

The momentum and energy equation then take the form

$$\frac{d\mathbf{q}_a}{dt} = -\sum_b \nu_b \left(\frac{P_a}{N_a^2} + \frac{P_b}{N_b^2} - \frac{Kv_{\rm sig}}{\overline{N}_{ab}}(\mathbf{q}_a^* - \mathbf{q}_b^*)\cdot\mathbf{j}\right)\nabla_a W_{ab} \tag{4.12}$$

and

$$\frac{d\hat{e}_a}{dt} = -\sum_b \nu_b \left(\frac{P_a\mathbf{v}_b}{N_a^2} + \frac{P_b\mathbf{v}_a}{N_b^2} - \frac{Kv_{\rm sig}}{\overline{N}_{ab}}(e_a^* - e_b^*)\mathbf{j}\right)\cdot\nabla_a W_{ab}. \tag{4.13}$$

If the gas is cold (u and P both zero) the contribution to dissipation of a from b in the momentum equation involves

$$\gamma_a^*\mathbf{v}_a\cdot\mathbf{j} - \gamma_b^*\mathbf{v}_b\cdot\mathbf{j}, \tag{4.14}$$

while the dissipation in the energy equation involves

$$\gamma_a^* - \gamma_b^*. \tag{4.15}$$

These terms are similar to the dissipation based on baryon scattering used by Amsden *et al.* [2] for a fluid dynamical simulation of nuclei collisions.

To determine an equation for the rate of change of thermal energy we write u in terms of $\mathbf{q}$ and $\hat{e}$,

$$u = \gamma(\hat{e} - \mathbf{v}\cdot\mathbf{q}) - 1. \tag{4.16}$$

By differentiating (4.16) we find

$$\frac{du}{dt} = -\frac{P}{N}\frac{d\gamma}{dt} + \gamma\frac{d\hat{e}}{dt} - \gamma\mathbf{v}\cdot\frac{d\mathbf{q}}{dt}, \tag{4.17}$$

which can be written

$$\frac{du_a}{dt} = -\left(\frac{P}{N}\frac{d\gamma}{dt}\right)_a + \frac{\gamma_a P_a}{N_a^2}\sum_b \nu_b\mathbf{v}_{ab}\cdot\nabla W_{ab} + \gamma_a K\sum_b \frac{\nu_b}{\overline{N}_{ab}}v_{\rm sig}[(e_a^* - e_b^*) - (\mathbf{v}_a\cdot\mathbf{j})(\mathbf{q}_{ab}^*\cdot\mathbf{j})]r_{ab}F_{ab}, \tag{4.18}$$

where the term multiplied by K is the dissipation. If the gas is cold (that is, we set u and P to zero) the dissipation term can be written

$$\gamma_a K\sum_b \left(\frac{\nu_b}{\gamma_a^*\overline{N}_{ab}}\right)v_{\rm sig}(1 - \gamma_{ab}^*)r_{ab}F_{ab}, \tag{4.19}$$

where γ_{ab}^* is calculated with the velocity of particles a relative to b along $\mathbf{j}$. This velocity is

$$v_{ab}^* = \frac{\mathbf{v}_a\cdot\mathbf{j} - \mathbf{v}_b\cdot\mathbf{j}}{1 - (\mathbf{v}_a\cdot\mathbf{j})(\mathbf{v}_b\cdot\mathbf{j})}. \tag{4.20}$$

Since $\gamma \geq 1$ and $F_{ab} < 0$ the dissipation is ≥ 0. This dissipation is the viscous dissipation of the cold gas. When the thermal terms are reintroduced, the nonrelativistic limit [24] shows that the thermal terms contribute to heat conduction and therefore may increase or decrease the internal energy of a parcel of fluid. The relationship between our dissipation terms and the entropy will be given elsewhere.

5. THE SIGNAL VELOCITY

The local eigenvalues for the relativistic one-dimensional Euler equations are $(v \pm c_s)/(1 \pm vc_s)$ and v. In finite difference solutions the appropriate signal velocities depend on the solution of a Riemann problem for the left and right states of the finite difference cells (see, for example, [27, 28] for the nonrelativistic case and [16, 17] for the relativistic case). In SPH simulations we can consider the particle a and the particle b as the left and right states. The one-dimensional Riemann problem is then taken with respect to motions along the line joining the two particles and the appropriate signal velocity is the speed of approach (as seen in the computing frame) of signals sent from a towards b and vice versa [22].

It is useful to recall how the non-relativistic signal veloc-

ity is estimated [22]. We begin by noting that the speed of sound associated with particle a (taking into account the new state) is approximately

$$c'_a = \sqrt{c_a^2 + \beta(\mathbf{v}_{ab}\cdot\mathbf{j})^2}, \tag{5.1}$$

where β is a parameter ~ 1. We can approximate (5.1) by

$$c'_a = c_a + |\mathbf{v}_{ab}\cdot\mathbf{j}|. \tag{5.2}$$

The signal velocity we need is the speed of approach of the signal sent from a to b and that from b to a as seen in the computing frame. The argument for this choice is that when information about the states meets it is time to construct a new state. It is precisely this relative speed which should be used in the Courant condition.

The component of the velocity of a along the line joining a to b is

$$v_a^* = -\mathbf{v}_a\cdot\mathbf{j}, \tag{5.3}$$

and the nonrelativistic signal velocity is then

$$v_{\text{sig}} = (v_a^* + c'_a) - (v_b^* - c'_b), \tag{5.4}$$

which can be approximated by

$$v_{\text{sig}} = c_a + c_b + 3v_{ab}^*, \tag{5.5}$$

where

$$v_{ab}^* = v_a^* - v_b^* = -\mathbf{v}_{ab}\cdot\mathbf{j}$$

is ≥ 0 for approaching particles. When the particles are not approaching, we turn the dissipation terms off and v_{sig} is not needed.

The reader might wonder why we do not solve the exact one-dimensional Riemann problem to determine the signal speed. As mentioned in the introduction our aim is to estimate simple robust approximations which do not depend on solving the Riemann problem for each new material. It is already known that, for nonrelativistic materials (including gases, liquids, and metals) that dissipative terms of the kind considered here give good results. We hope to achieve that universality with the dissipation being considered.

To generalize these results to the relativistic case we first need to estimate the speed of sound equivalent to (5.1) or (5.2). We are unaware of good estimates of the speed of sound comparable to (5.1) and there are infinitely many choices which reduce to (5.1) in the nonrelativistic limit. In this paper therefore we confine ourselves to simple approximations which, remarkably, lead to quite good results. In the first of these we replace (5.2) by

$$c'_a = \frac{c_a + |v_{ab}^*|}{1 + c_a|v_{ab}^*|}, \tag{5.6}$$

with a similar expression for c'_b. This approximation, although rather crude, has the right non-relativistic limit and provides a reasonable bound on the effective speed of sound. Our first signal speed is then defined to be

$$v_{\text{sig}}^{(1)} = \frac{c_a + |v_{ab}^*|}{1 + c_a|v_{ab}^*|} + \frac{c_b + |v_{ab}^*|}{1 + c_b|v_{ab}^*|} + |v_{ab}^*|. \tag{5.7}$$

The second form for v_{sig} is based on the speed of sound produced when two cold streams collide at ultra relativistic speeds. When the cold gas is shocked its thermal energy jumps to $(\gamma - 1)$, where γ is calculated with the relative velocity of the pre- and postshocked states. We simply add a term of this form to the thermal energy in the definition of the speed of sound of a relativistic gas. The effective speed of sound for particle a then has the form

$$c'_a = \left(\frac{c_a^2 + \beta(\gamma_{ab}^* - 1)}{1 + (c_a^2 + \beta(\gamma_{ab}^* - 1)/(\Gamma - 1))}\right)^{1/2}, \tag{5.8}$$

where γ_{ab}^* (defined after (4.19)) is the γ calculated using the component of the velocity of a relative to b along $\mathbf{j}$ and Γ is the adiabatic index (see (7.1). This form of the effective speed of sound is a natural generalization of (5.1) and it has the correct relativistic limit (when γ_{ab}^* is infinite and $\Gamma = \frac{4}{3}$) and the correct nonrelativistic limit.

As in the nonrelativistic case we construct the signal velocity by determining the speed with which sound waves from a to b and vice versa approach according to an observer at rest in our computing frame. This is given by subtracting the signal velocities to give what we have called v_{sig}. We do not calculate the velocity of one propagating signal relative to the other but simply subtract the signals since this tells us when the states need to be recomputed. Our second signal velocity is then

$$v_{\text{sig}}^{(1)} = \frac{c'_a + v_a^*}{1 + c'_a v_a^*} - \frac{v_b^* - c'_b}{1 - c'_b v_b^*}. \tag{5.9}$$

Since Schneider *et al.* [25] have found that their results do not depend sensitively on approximations to the signal velocities and nonrelativistic SPH simulations are not sensitive to the approximations, we expect (and it is borne out by the calculations for gases) that these signal speeds will give similar results.

The parameter K has not yet been specified. In the absence of other information we choose $K = 0.5$, since this is the value found to work for the nonrelativistic simulations. We find that it leads to satisfactory results.

Finally we note that, unlike finite difference Eulerian codes, we do not include any signal based terms in the continuity equation. They are unnecessary for SPH.

6. THE TIME STEP

The local Courant condition is

$$\delta t_c = \frac{\Delta}{v_{\text{sig}}}, \tag{6.1}$$

where Δ is a distance related to the separation of the particles. In the calculations to be described here the particles have an $h \propto 1/N$ and therefore approximately proportional to the particle separation. It is not exactly proportional because N is a smoothed density. However, in order to work out the rates of change, we use a symmetric h for the interaction between two particles given by $h = (h_a + h_b)/2$, and this can differ significantly from the local particle separation. We have experimented with replacing Δ by both the symmetric form of h and by the separation of the interacting particles. In general the results are very similar with the exception of the wall shock problem where using the particle separation gave absurdly small time steps.

The Courant time step control uses the minimum of (6.1) over all particles. In addition to a time step control based on the Courant condition we also use a time step based on the rate of change of q. This time step control was introduced for astrophysical problems where body forces would occur. Denoting the rate of change of $\mathbf{q}$ by $\mathbf{f}$ the time step takes the form

$$\delta t_f = (\sqrt{h/|\mathbf{f}|}), \tag{6.2}$$

where the minimum of δt_f is taken over all particles. In our computations we use the minimum of δt_c and δt_f. We find they give a very similar time step control, except for the early stages of some computations when δt_f gives a smaller time step.

7. SOLVING FOR P AND V

Following [17] we determine P, v, and u by rewriting the equation of state as a function of P alone, using the values of N, q, and $\hat{e}$ from the integration of the equations of motion to express u, and γ as functions of P. In this paper the equation of state is

$$P = (\Gamma - 1)nu, \tag{7.1}$$

which can be written as a function of P by noting from (4.16) that

$$u = \frac{\hat{e}}{\gamma} + \frac{P(1-\gamma^2)}{N\gamma} - 1, \tag{7.2}$$

and from (2.8) and (2.9),

$$\gamma = 1/\sqrt{1 - q^2/(\hat{e} + P/N)^2}. \tag{7.3}$$

At the end of the step (or after a predictor step) we have new values of q, N, and $\hat{e}$. With these values (7.3) defines γ as a function of P. Substituting for γ into (7.2) gives u as a function of P. Finally, substituting these quantities into (7.1), and replacing n by N/γ converts (7.1) into a nonlinear equation for P which we solve using the Newton–Raphson method.

8. NUMERICAL TESTS

In the following experiments we integrate the acceleration, energy, and continuity equations using a second-order predictor–corrector method. The numerical integration conserves total energy and momentum to within the roundoff error (10^{-17} for these calculations).

In all cases the resolution length h for the kernels was allowed to vary with density according to the rule $h \propto 1/N$. When calculating the kernels and their derivatives we use the average $h = 0.5(h_a + h_b)$. The initial value of h_a was 1.5 the initial particle spacing at the position of particle a. We use the cubic spline kernel [20].

Discontinuities in the initial u and N were smoothed according to the rule

$$A = \frac{A_L + A_R e^{x/d}}{1 + e^{x/d}}, \tag{8.1}$$

where A_L denotes the uniform state to the left of the origin, A_R denotes the uniform state to the right of the origin, and d is taken as half the largest initial particle separation at the interface. The SPH simulations are more consistent with smoothing the initial conditions with the kernel. In the present case this presents some problems because the h we choose for each particle depends on the density which in turn will depend on the smoothing and therefore on the h. The crude but simple smoothing (8.1) gives satisfactory results but we are aware that it can hardly be the optimum way to smooth the initial conditions.

Since we use SPH particles with equal numbers of baryons higher densities are associated with closer particle spacing and, if the initial density is discontinuous, and it is smoothed according to (8.1), the particle spacing and the initial h must also be smoothed. In the case of the shock

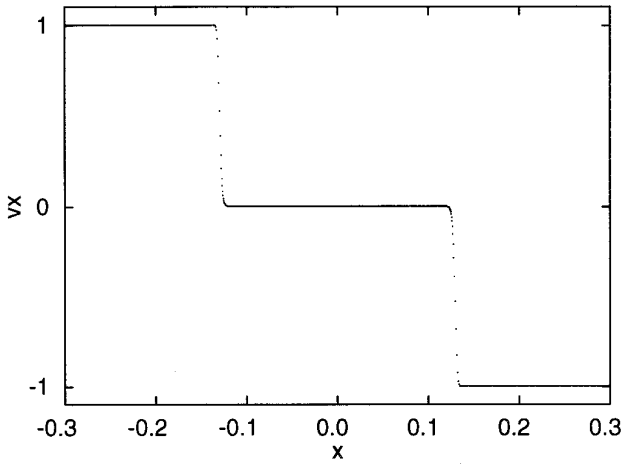

FIG. 1. Velocity against distance for the two cold colliding streams each with speed 0.9999. Details are given in the text.

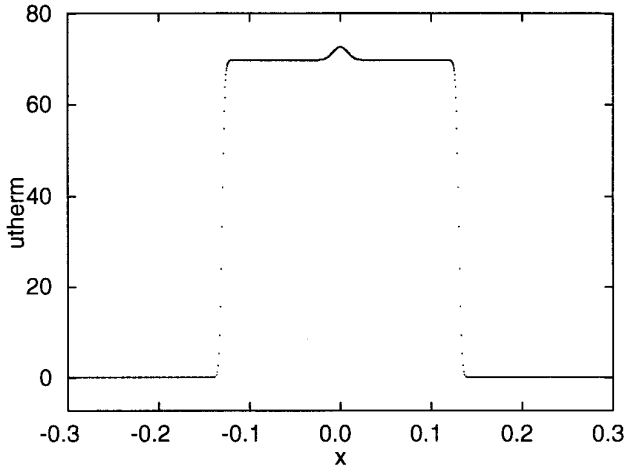

FIG. 3. Number density N against distance for the colliding streams.

tube, for example, the spacing changes by a factor of 10 across the initial interface and, if this is not smoothed, the evolution is very badly corrupted. This might be expected since SPH is based on smoothing the equations of motion.

The particles are spaced according to the rule

$$\rho_{a\frac{1}{2}}(x_{a+1} - x_{a-1}) = \rho_R \Delta_R, \tag{8.2}$$

where ρ_R is the density of the fluid to the far right of the origin where the particle spacing is Δ_R.

Wall Shock

In Figs. 1 to 3 we show the result of two identical cold streams of gas with $\Gamma = \frac{5}{3}$ colliding. The initial conditions are $N = 1$, $u = 10^{-6}$ and the speed of each stream is 0.9999. The initial particle spacing is 0.001 and $v_{\text{sig}}^{(1)}$ is used. The time step is based on $\Delta = (h_a + h_b)/2$.

The velocity profiles in Fig. 1 show no sign of oscillation and the shock is spread over about three initial particle spacings. In common with the nonrelativistic SPH calculations for the wall shock the thermal energy and the density have an error of a few percent at the interface (the error in the number density is larger) but the postshock values have errors of only 0.2%. These results agree well with those of Schneider *et al.* [25], although their RHHLE method gives better results at the interface. Very similar results were obtained using $v_{\text{sig}}^{(2)}$.

Blast Wave

In Figs. 4 to 7 we show the results for the blast wave simulated by Martí and Müller [17]. The initial configura-

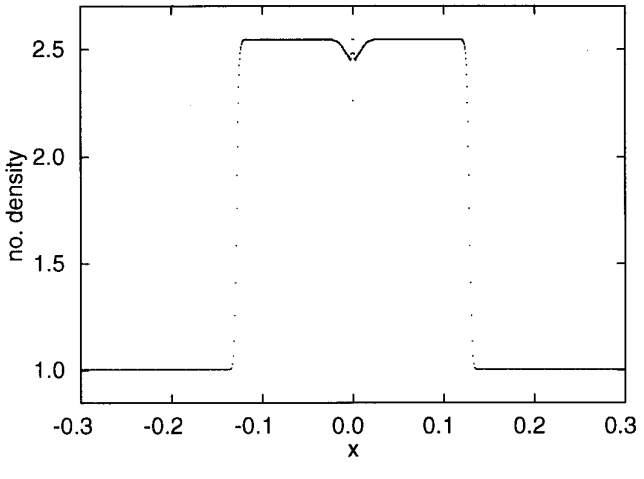

FIG. 2. Thermal energy u against distance for the colliding streams.

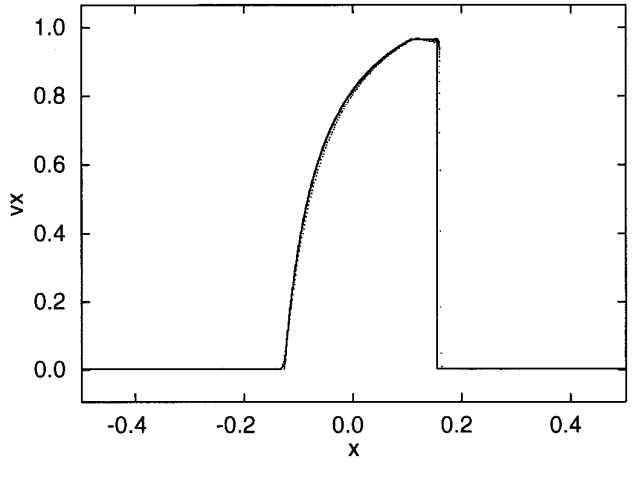

FIG. 4. Velocity against distance for the blast wave. Details are given in the text.

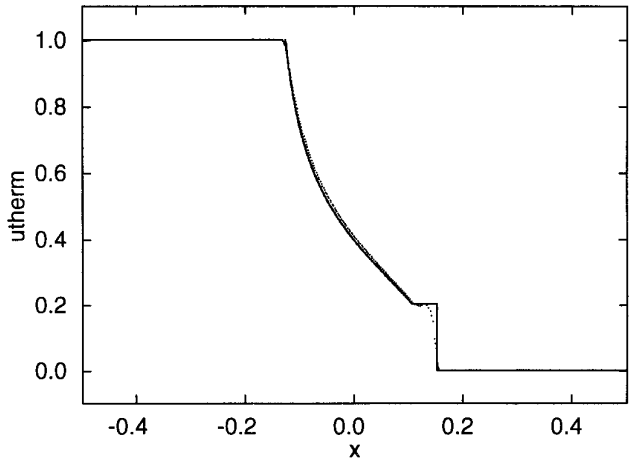

FIG. 5. Thermal energy for the blast wave.

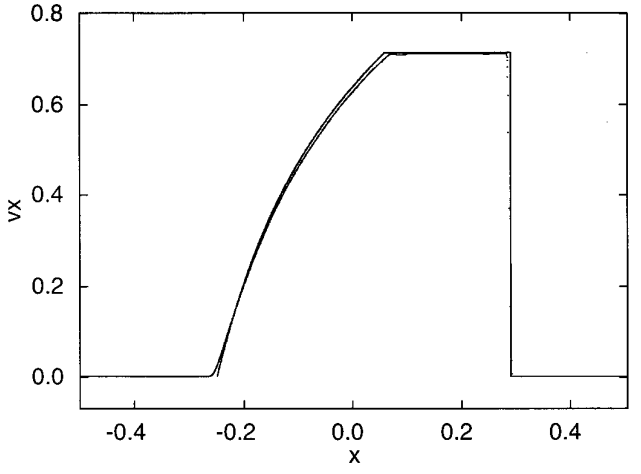

FIG. 8. Velocity against distance for the shock tube. Details are given in the text.

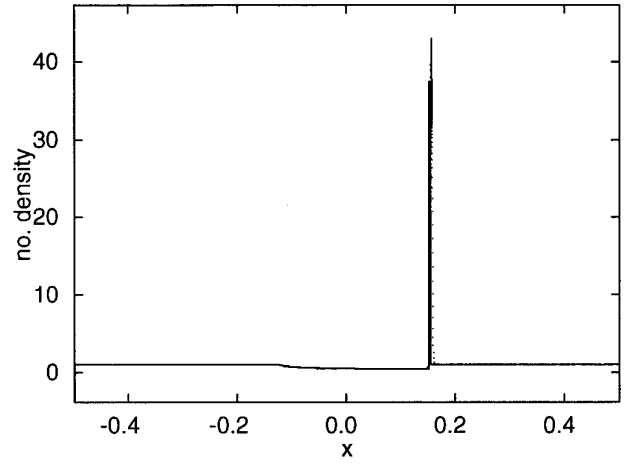

FIG. 6. Number density N against distance for the blast wave.

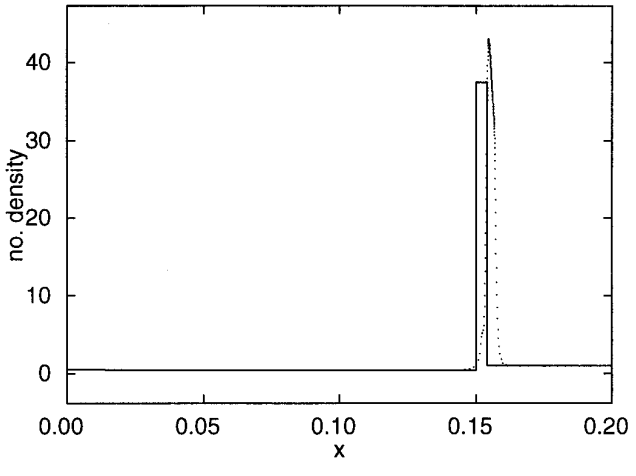

FIG. 7. Details of the number density spike for the blast wave.

tion consists of a static gas with $\Gamma = \frac{5}{3}$. To the left of the initial interface, $N = 1$ and $P = 1000$, while to the right of the interface, $N = 1$ and $P = 0.01$. The particle spacing is 0.001 and we use $v_{\text{sig}}^{(2)}$ and a time step based on $\Delta = (h_a + h_b)/2$. The velocity profile is smooth and the shock is spread over about three initial particle spacings. There are several particles in the shock profile but this is due to the density jumping by a factor 40 and the particle spacing decreasing by $\sim$40. The thermal energy shown in Fig. 5 is excellent, except for the smoothing near the shock front. The density profile in Fig. 6 shows the characteristic spike which makes this a difficult problem. The SPH calculation is very good except for an overshoot of the spike. In Fig. 7 we show the spike in more detail. It can be seen that apart from the overshoot the SPH simulation overestimates the shock speed by $\sim$2%. These results are in good agreement with those of Martí and Müller [17] and Martí *et al.* [15] who also find that significant errors occur in the spike (our errors are smaller but they use only 400 cells). Similar results were obtained using $v_{\text{sig}}^{(1)}$ and a time step based on Δ equal to the spacing of the two interacting particles.

Shock Tube

In Figs. 8 to 10 we show results for the shock tube simulated by Martí and Müller [17]. The initial configuration consists of a static gas with $\Gamma = \frac{5}{3}$. To the left of the interface $N = 10$ and $P = \frac{40}{3}$. To the right of the interface $N = 1$ and $P = 10^{-6}$. The particle spacing to the right of the interface is 0.005 and, because we use SPH particles with an equal number of baryons, the spacing to the left of the interface is 0.0005. The density and the spacing are smoothed according to (8.1).

We use $v_{\text{sig}}^{(1)}$ and a courant time step based on $\Delta = (h_a + h_b)/2$. The velocity profile in Fig. 8 shows very slight

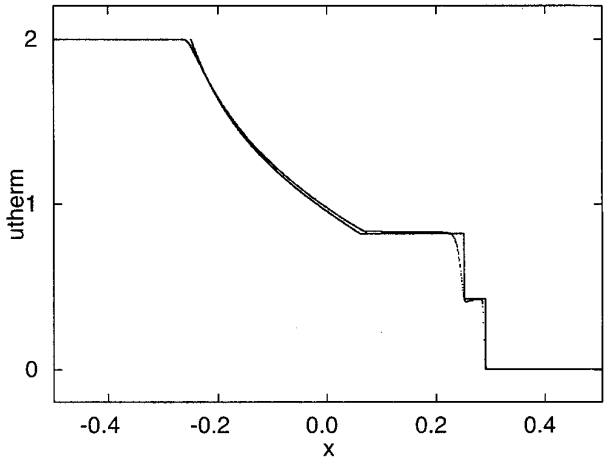

FIG. 9. Thermal energy against distance for the shock tube.

oscillations but, overall, the results are good. The thermal energy profile in Fig. 9 shows the effect of excessive thermal diffusion around the contact discontinuity. In the case of strong nonrelativistic shocks this thermal diffusion was reduced by defining e^* with reduced thermal energy [22] but in the relativistic case it is not clear how to do this consistently. The pressure profile in Fig. 10 shows that the pressure is constant between the rarefaction and the leading shock front.

Compared to the results obtained by Schneider *et al.* [25] our results are substantially better than those from the SHASTA code and comparable to those with RHHLE and LCPFCT. It is difficult to make an entirely fair comparison between the finite difference methods and SPH for these calculations because our particles enter the shock with a resolution (0.005) which is the same as Schneider *et al.* but poorer than that of Martí and Müller (0.0025), but in the rarefaction we initially have a much better resolution (0.0005) which then ranges between 0.0005 and 0.001 as the system evolves.

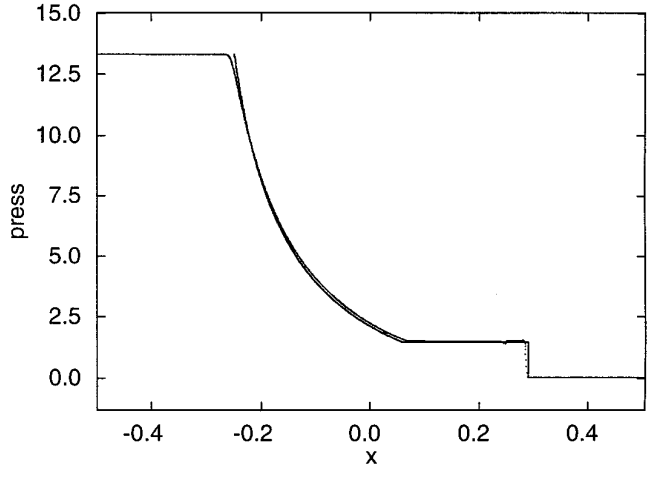

FIG. 10. Pressure for the shock tube.

9. DISCUSSION

The ultra relativistic SPH algorithm described in this paper gives good results for the ideal relativistic gas in shock tubes and similar configurations. Carefully tuned Riemann solvers give more accurate results for the same resolution but SPH has the advantage that it can be made adaptive almost trivially, and it can be extended easily to configurations involving more complicated physics.

Improvements can be expected in the way $v_{\rm sig}$ is determined, although the simulations described here indicate a remarkable tolerance to its precise form. The evaluation of the density from the continuity equation is clearly adequate for quite extreme conditions. In addition to the simulations described here we also simulated the expansion of a relativistic gas into a vacuum to check that low density regions would be simulated satisfactorily. We have not yet experimented with the strong rarefactions which would be expected in the relativistic version of the Sjögreen test, where two regions of gas move away from each other. The problems which might arise would be due to errors in the integration of the continuity equation in the form (3.1) which might lead to the fatal error of negative density. This problem could be controlled easily either by using, in place of (3.1),

$$\frac{dN_a}{dt} = N_a \sum_b \frac{\nu_b}{N_b} \mathbf{v}_{ab} \cdot \nabla_b W_{ab}, \tag{9.1}$$

which can be easily integrated for $\log N_a$, after which N_a can be recovered in a positive definite form. Alternatively, N_a can be found by the usual SPH summation formula which guarantees that the density is positive definite.

The extension of our algorithm to two or more dimensions is trivial since vector quantities have been used. The determination of those particles which contribute to a given particle's properties is, however, more difficult because each particle has its own h. In astrophysical calculations tree codes are used since they are used to calculate the gravitational forces. For a pure fluid dynamical simulation it would be preferable to use rank lists.

REFERENCES

1. C. E. Akujor, *Astron. Astrophys.* **259,** L61 (1992).
2. A. A. Amsden, A. S. Goldhaber, F. H. Harlow, and J. R. Nix, *Phys. Rev. C* **17,** 2080 (1978).
3. R. B. Clare and D. Strottmann, *Phys. Rep.* **137,** 277 (1986).
4. P. Collela and H. M. Glaz, *J. Comput. Phys.* **59,** 264 (1985).
5. R. Donat and A. Maquina, *J. Comput. Phys.* **125,** 42 (1996).

6. G. C. Duncan and P. A. Hughes, *Ap. J.* **436,** L119 (1994).
7. C. Eckart, *Phys. Rev.* **58,** 919 (1940).
8. B. Einfeldt, C. D. Munz, P. L. Roe, and B. Sjorgreen, *J. Computat. Phys.* **92,** 273 (1991).
9. S. A. E. G. Falle and S. S. Komissarov, *Mon. Not. Roy. Astro. Soc.* **278,** 586 (1996).
10. W. A. Hiscock and L. Lindblom, *Phys. Rev. D* **31,** 725 (1985).
11. W. Israel, *Covariant Fluid Dynamics and Thermodynamics*, Relativistic Fluid Dynamics, edited by A. Anile and Y. Choquet-Bruhat, (Springer-Verlag, New York/Berlin, 1987) p. 152.
12. P. Laguna, W. A. Miller, and W. H. Zurek, *Ap.J.* **404,** 678 (1993).
13. L. D. Landau and E. M. Lifshitz, *Fluid Mechanics* (Pergamon, Elmsford, NY, 1987).
14. P. J. Mann, *Comp. Phys. Comm.* **67,** 245 (1991).
15. J. Mª. Martí, J. M. Ibánēz, and J. A. Miralles, *Phys. Rev. D* **43,** 3794 (1991).
16. J. Mª. Martí and E. Müller, *J. Fluid Mech.* **258,** 317 (1994).
17. J. Mª. Martí and E. Müller, *J. Comput. Phys.* **123,** 1 (1996).
18. J. Mª. Martí and E. Müller, J. Mª. Ibánez, *Astron. Astrophys.* **281,** L9 (1994).
18. J. Mª, Martí and E. Müller, J. Mª. Ibánez, *Astron. Astrophys.* **281,** L9 (1994).
19. J. Mª. Martí and E. Müller, J. A. Font, and J. Mª. Ibánez, *Ap. J.* **448,** L105 (1995).
20. J. J. Monaghan, *Annu. Rev. Astron. Astrophys.* **30,** 543 (1992).
21. J. J. Monaghan, *Relativistic SPH;* Mathematics Dept., Monash University, 1994.
22. J. J. Monaghan, *SPH and Riemann solvers, J. Comput. Phys.* 1996. [submitted]
23. M. L. Norman and K.-H. Winkler, *Astrophysical Radiation Hydrodynamics* edited by Norman and Winkler, (Reidel, Dordrect, 1986).
24. T. S. Olson and W. A. Hiscock, *Phys. Rev. D.* **41,** 3687 (1990).
25. V. Schneider, U. Katscher, D. H. Rischke, B. Waldhauser, J. A. Maruhn, and C. D. Munz, *J. Comput. Phys.* **105,** 92 (1993).
26. C. W. Schultz-Rinne, J. P. Collins, and H. M. Glaz, *SIAM J. Sci. Statist. Comput.* **14,** 1394 (1993).
27. E. G. Toro, *Phil. Trans. A. R. Soc.* **341,** 499 (1992).
28. Whitehurst, *Mon. Not. Roy. Astr. Soc.* **277,** 655 (1995).
29. K. Xu, L. Martinelli, and A. Jameson, *J. Comput. Phys.* **120,** 48 (1995).
30. K. Xu, K. Chongam, L. Martinelli, and A. Jameson, BGK-based schemes for the simulation of compressible flow, *Int. J. Comp. Fluid. Dyn.* (1996).